Polymer Testing 157 (2026) 109138

Contents lists available at ScienceDirect

Polymer Testing

journal homepage: www.elsevier.com/locate/polytest

A predictive rheological framework to define printability of thermo-sensitive bioinks using non-temperature-controlled bioprinters

Inês Anjos [a,b], Tânia Vieira [a,b,c], Luana Ventura [a,b], Taslima Aktar [a,b], Jorge Carvalho Silva [a,b,c], Bárbara B. Mendes [d], João Conde [d], Luis Felipe Bolaños [e], Susete Fernandes [a,b], Catarina Leal [b,f,g], João Paulo Borges [a,b], David Limón [a,b,*]

[a] Department of Materials Science NOVA School of Science and Technology, Caparica, Portugal
[b] CENIMAT/I3N NOVA School of Science and Technology, Caparica, Portugal
[c] Physics Department NOVA School of Science and Technology, Caparica, Portugal
[d] Comprehensive Health Research Centre (CHRC), NOVA Medical School, Universidade NOVA de Lisboa, Lisbon, Portugal
[e] Department of Economics NOVA School of Business and Economics, Portugal
[f] Physics Department, Instituto Superior de Engenharia de Lisboa, Instituto Politécnico de Lisboa, Lisbon, Portugal
[g] CeFEMA, Instituto Superior Técnico, Universidade de Lisboa, Portugal

ARTICLE INFO

Keywords:
Tissue engineering
3D bioprinting
Bioinks
Printability
Hydrogels
Rheology
Biocompatibility

ABSTRACT

3D-bioprinting requires bioinks with a set of mechanical and chemical characteristics, including biocompatibility, suitable flow, the preservation of cell viability during extrusion, and shape retention upon printing to construct structures in 3D. Biopolymer-based hydrogels including mixtures of gelatin and alginate are ideal, although their printability is challenging due to important thermoresponsive behavior, requiring expensive temperature-controlled printers.

Here, we present a methodological framework that predicts the printability of gelatin–alginate bioinks directly from rheological parameters. By quantitatively linking viscosity and storage/loss ratio to extrusion fidelity, and by identifying gelation temperature and gelation speed as key windows for adjusting the printing process, we establish actionable design rules that enable printing with non-temperature-controlled devices, resulting in shape fidelity, spreading ratios, and printability ratios close to 1, while permitting a high cell viability after printing (92.4 ± 2.2%) that can be maintained for up to 8 days (96.5 ± 0.9%).

This predictive approach provides a practical pathway to design thermosensitive bioinks without relying on trial-and-error or specialized equipment, broadening the accessibility of 3D bioprinting technologies for tissue engineering.

1. Introduction

3D bioprinting is a key technique in tissue engineering, as it enables the fabrication of biomimetic structures with high spatial resolution and provides valuable insights into cell–cell interactions and drug screening [1–4]. Its success depends on the use of bioinks that meet strict requirements to ensure both printability and functionality of the printed constructs. Bioinks must exhibit biocompatible chemistry; possess viscoelastic properties that allow precise deposition while minimizing shear stress-induced cell damage; stabilize upon deposition to form complex 3D structures; maintain integrity under physiological culture conditions; and permit efficient diffusion of nutrients and waste products to sustain cell survival and function [5].

Hydrogels are especially suited for this purpose, as they behave as solids despite containing more than 90% solvent [6,7]. Biopolymer-based hydrogels are particularly attractive candidates because their water-rich structure and biochemical cues mimic the extracellular matrix (ECM), supporting cell adhesion, proliferation, and differentiation. Moreover, their physicochemical properties can be tuned to influence cell behavior [8–10]. Among these, gelatin—derived from collagen—offers biocompatibility and integrin-binding sites, and undergoes reversible gelation near room temperature, providing structural integrity [9,11]. Alginate, a polysaccharide extracted from seaweed, is also widely used due to its biocompatibility and ability to

* Corresponding author. Department of Materials Science NOVA School of Science and Technology, Caparica, Portugal.
E-mail address: davidlimon@fct.unl.pt (D. Limón).

https://doi.org/10.1016/j.polymertesting.2026.109138
Received 3 September 2025; Received in revised form 20 January 2026; Accepted 3 March 2026
Available online 12 March 2026

form ionically crosslinked networks in the presence of divalent cations [8,12–15].

Combining alginate with gelatin has attracted considerable interest, as the mixture combines the benefits of both polymers: high biocompatibility, tunable viscoelastic properties, and the possibility of ionic crosslinking to stabilize constructs under physiological conditions despite gelatin's thermoreversible nature [8,9,15–19]. However, gelatin's gelation and rheological properties are highly temperature-dependent [11], requiring precise temperature control during bioprinting [19–23]. This dependence poses a challenge, as temperature-controlled printers are expensive, limiting the accessibility of gelatin- and other thermosensitive-based bioinks. Most studies using gelatin–alginate inks have relied on trial-and-error optimization of printing conditions (e.g., speed, needle diameter, or pressure), and assessed printability through indicators such as fiber continuity, spreading ratio, layer stacking, shape fidelity, and printability ratios. Giuseppe et al. [24] evaluated gelatin–alginate inks on a non-temperature-controlled printer, but assumed constant bioink temperature throughout the process, overlooking its impact on printability.

Few authors attempted to correlate rheological properties with printability. Chung et al. [19] pointed the need of a solid-like behavior (G'>G″) for a good printability, whereas Paxton et al. [23] pointed yield stress, shear thinning, and recovery tests qualitatively as tools to select a bioink with better printability. Gao et al. [16] found that the extrusion pressure depends on G′ and G″ collectively, and suggested that good printability requires bioinks with loss factor values (G''/G') between 0.25 and 0.45. However, all these works used bioprinters with active temperature control, keeping the bioink at a constant temperature, they consider very few gelatin-alginate mixtures, and do not study in detail the influence of temperature. Table 1 lists relevant works studying the influence of rheological parameters on printability of gelatin-alginate bioinks as well as the predictive/descriptive nature of the contribution.

Here, we address a critical gap in the field: despite the extensive literature on gelatin–alginate bioinks—including influential studies that relate rheological properties to printability—most approaches optimize printing at a single, fixed temperature using printers with active thermal control. Consequently, printability remains largely tuned by trial-and-error within narrowly defined conditions, which limits reproducibility, hampers transferability across laboratories, and constrains implementation on low-cost bioprinters lacking temperature regulation. In contrast to prior work that correlates rheological parameters with printability at one selected temperature, we introduce a predictive framework that explicitly accounts for the temperature dependence of viscoelastic behavior. By systematically mapping viscosity and the elastic-to-viscous balance (G′/G″) across temperature and linking these variables to semi-quantitative printability metrics, we identify rheological windows that anticipate successful printing rather than retrospectively describing it (Fig. 1).

Importantly, our framework extends beyond static temperature setpoints by incorporating a temporal dimension: we define a room-temperature printing time window governed by cooling and gelation kinetics. This enables controlled and reproducible printing without active thermal control, a condition not addressed in previous gelatin–alginate studies.

The framework is validated using quantitative printability metrics—including spreading, printability ratio, shape fidelity, height fidelity, and height stability—and through the fabrication of a composite 3D structure assembled from two bioinks in three sequential printing stages. These results demonstrate that temperature-dependent rheological mapping can be translated into stable multilayer builds and geometrically complex constructs under non-temperature-controlled conditions, moving gelatin–alginate bioprinting from descriptive optimization toward predictive design. Importantly, we demonstrate the construction of breast cancer tissue models, which remain viable for several days. This optimization could broaden the applicability of gelatin and other thermosensitive bioinks in tissue engineering.

2. Results and discussion

2.1. Solubility and manual extrusion

As a first screening, alginate (0.1–10 % w/v), gelatin (0.1–10 % w/v) and their mixtures were dissolved in PBS to mimic physiological pH and ionic strength. Table S 1 in the Supporting Information summarises the concentrations tested and whether they dissolved. Formulations were named according to their alginate and gelatin contents (e.g., **A1G3** contains 1 % alginate and 3 % gelatin). Alginate provides carboxylate groups, while gelatin contains guanidine (arginine), amino (lysine) and imidazole (histidine) groups. Although all these functional groups ionize near neutral pH, gelatin dissolved readily (<1 h) throughout the tested range, but alginate was insoluble above 5 % (**A5G0** to **A5G7**), whereas mixtures with ≥3 % alginate dissolved more slowly (>1 h) because of the polymers' high molecular weight (gelatin 50 000–100 000 g/mol; alginate 10 000–600 000 g/mol).

Table 1
Gelatin–alginate printability: prior studies by temperature control, rheology, assessment, and predictive scope.

Study (year)	Temperature control	Alg–Gel compositions	Rheology considered	Printability assessment	Predictive scope	Ref
Chung et al., 2013	Yes (controlled setpoints)	Alg–Gel blends	Viscosity, G′/G″; temperature effects qualitatively	Qualitative print quality; resolution/precision	Descriptive	[19]
Paxton et al., 2017	Yes	Multiple inks incl. Alg–Gel	Yield stress, shear-thinning, recovery (protocolized)	Filament formation - rheology screen	Heuristic/ descriptive	[23]
Ouyang et al., 2016	Yes	Gelatin/alginate variants	None (focus on image metric)	Printability index on lattices $Pr = L^2/16A$	Metric only	[20]
Ribeiro et al., 2017	Yes	Generic hydrogels	G′/G″ moduli and yield stress as a function of composition	Filament collapse & fusion (quantitative image analysis)	Methodological	[25]
Gao et al., 2018	Yes (single T)	Gelatin–alginate composites	G′, G″; tan δ ≈ 0.25–0.45	Pressure/printability at fixed T	Semi-predictive at one T	[16]
Di Giuseppe et al., 2018	Usually controlled; no systematic T-mapping	Alg–Gel blends	Viscosity & mechanics emphasis	Lattice fidelity/accuracy; mechanical tests	Descriptive	[24]
Soltan et al., 2019	Yes	ADA–Gel (Alg derivative)	G′/G″; tan δ	Quantitative printability & viability	Semi-predictive	[12]
Gregory et al., 2022	Yes	One Alg–Gel composition (prepared with alginate of two MW); varying cell density	Viscoelasticity vs cell loading	Line spreading; viability; pressure	Descriptive with biological factors	[26]
Ahmadi-Soufivand et al., 2023	Yes (pre-cooling; setpoints)	Alg–Gel	Rheology-guided parameter tuning	Multilayer mesostructures	Descriptive optimization	[27]

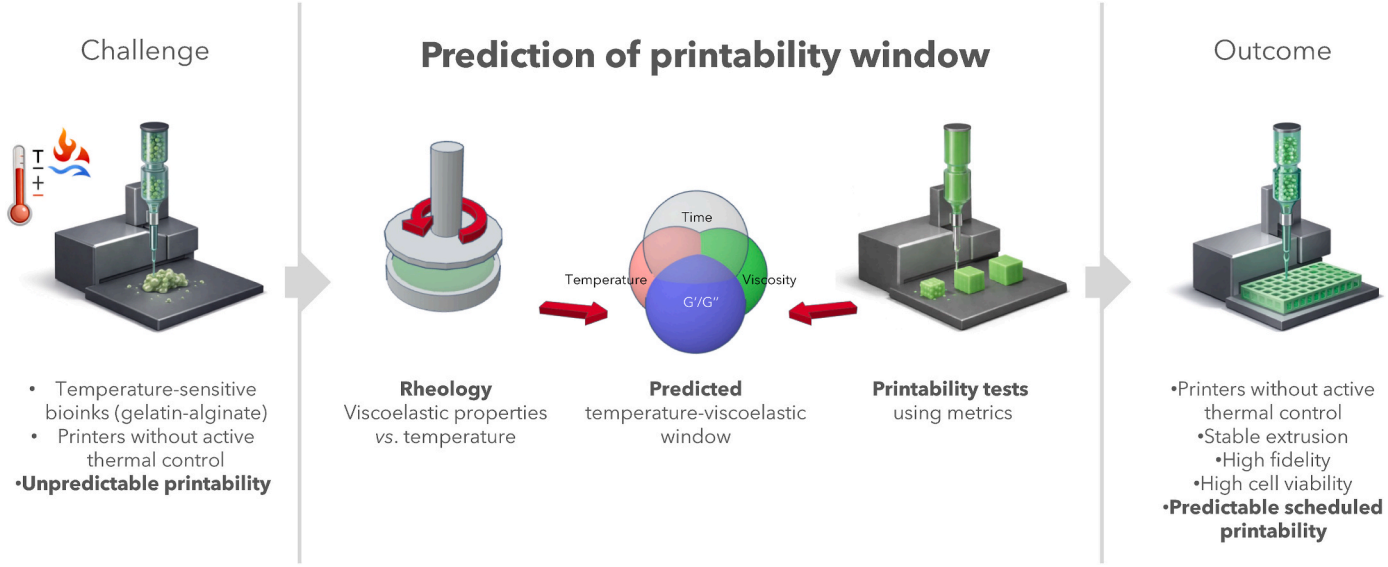

Fig. 1. Rheology-based predictive framework for the printability of thermosensitive bioinks in non-temperature-controlled bioprinting systems. Schematic overview of the methodology proposed. Thermosensitive gelatin–alginate bioinks printed using bioprinters without active temperature control often exhibit unpredictable printability due to uncontrolled thermal variations. By characterizing the temperature-dependent viscoelastic properties of the bioinks and accounting for time-dependent cooling kinetics, a predicted temperature–viscoelastic printability window can be defined, enabling the anticipation and scheduling of stable extrusion, high geometric fidelity, and preserved cell viability, without the need for active thermal regulation.

As a bioink requires to be extruded under a relatively low shear stress to protect the cells from lysis [20,28], we manually extruded the solutions through a syringe at 35, 30, 25 and 20 °C and assessed their macroscopic phase and relative ease of extrusion (Table S 1). Representative images are shown in Figure S 1. Higher polymer concentrations yielded more solid materials; temperature had little effect on alginate solutions but affected gelatin, which solidified as temperature fell. Fluid compositions (e.g., most pure alginate solutions, gelatin <3 % or low-concentration mixtures) were easy to extrude (level 1, similar to water) but lost their shape and are unsuitable for 3D printing. Highly concentrated formulations that were solid at ≥ 25 °C maintained shape but required high extrusion pressures (level 4, equivalent to a hard toothpaste), which could potentially damage cells (e.g., **A3G7**). Suitable bioinks extruded under low to medium pressure (levels 1–3) and kept their shape (semi-solid and solid at ≤ 25 °C); this occurred in gelatin solutions ≥5 % and mixtures with ≤3 % alginate and 5–7 % gelatin.

Later, crosslinking is necessary to maintain structure of printed constructs as they must be later incubated near 37 °C for cell survival, and gelatin becomes fluid at this temperature [20]. Divalent cations such as Ca^{2+} bind adjacent alginate chains and form a solid shell [19,29]. Accordingly, extruded hydrogels were immersed in 100 mM $CaCl_2$ for 1 min. Crosslinking stiffened the surface without altering the shape (Figure S 1).

On the basis of these results, formulations containing 0.66, 1 or 2 % alginate and 5, 6 or 7 % gelatin were selected for rheological tests (temperature and shear rate ramps) to study their viscoelastic behavior, including the liquid–solid transition and stiffness.

2.2. Gelation and strength

Analogous to crystallization, gelation involves the arrangement of gelator molecules into a network that entraps solvent, decreases entropy and kinetic energy compared to the solution, and releases energy to the surroundings (exothermic process) [6,30–32]. Cooling reduces molecular mobility and promotes supramolecular interactions (e.g., hydrogen bonds) between biopolymers and water, leading to a network with higher resistance to deformation.

To study this transition, the storage modulus (G′, elastic behavior) and loss modulus (G″, viscous behavior) of gelatin (5–7%), alginate (0.66–2%), and mixtures were measured during temperature ramps from 40 to 20 °C at −1 °C/min, with a constant frequency of 1 Hz and strain of 0.5% (within the linear viscoelastic region). Results for alginate and gelatin are shown in Fig. 2 A, while the mixtures are shown in the Supporting Information (Figure S 2).

Higher polymer concentrations increased both G′ and G″ by several orders of magnitude. Alginate solutions consistently exhibited viscous-dominated behavior (G″ > G′), unaffected by temperature. In contrast, gelatin solutions underwent gelation below ~27 °C, where G′ surpassed G″, indicating a transition to solid-like behavior. The Storage/loss ratio (G′/G″) (inverse loss tangent) describes this predominance of elastic over viscous response, and reflects the status of the gelation (Fig. 2 B). Its slope versus temperature reflects gelation speed (Fig. 2C). The gelation temperature (T_{gel}) is defined as the point where G′ = G″ (G′/G″ = 1) (Fig. 2 B), with values summarized in Fig. 2 D.

As observed, higher biopolymer concentrations led to a higher resistance to deformation (G′ and G″ values between 10 and 1000 Pa). Nonetheless, alginate solutions always show a predominant viscous component (fluid-like behavior) (G''>G′), which is not affected by temperature. In contrast, gelatin solutions undergo gelation, as observed by a crossover of the Storage over the Loss values (G'>G″) at lower temperatures (<27 °C), leading to a predominant elastic component (solid-like behavior).

Increasing gelatin concentration generally raised T_{gel}, consistent with the greater number of supramolecular interactions (hydrogen bonds, electrostatic interactions) that stabilize the network and require higher temperatures to disrupt. Adding alginate induced earlier gelation at higher temperatures than gelatin alone, reflected in increased G′ and G″ values (Figure S 2) and higher G′/G″ ratios above T_{gel} (Fig. 2 B). This effect raised T_{gel} at low alginate content (0.66%) but decreased it as alginate increased to 2% (Fig. 2 D), likely due to steric hindrance. At any given temperature, higher gelatin content yielded larger resistance to deformation, although at the T_{gel} of each composition (G′ = G″), values were similar across gelatin concentrations. Similarly, increasing alginate up to 2% also raised the resistance to deformation by several orders of magnitude at any given temperature (Fig. 2C), highlighting the strong influence of additional supramolecular interactions created by alginate in the network.

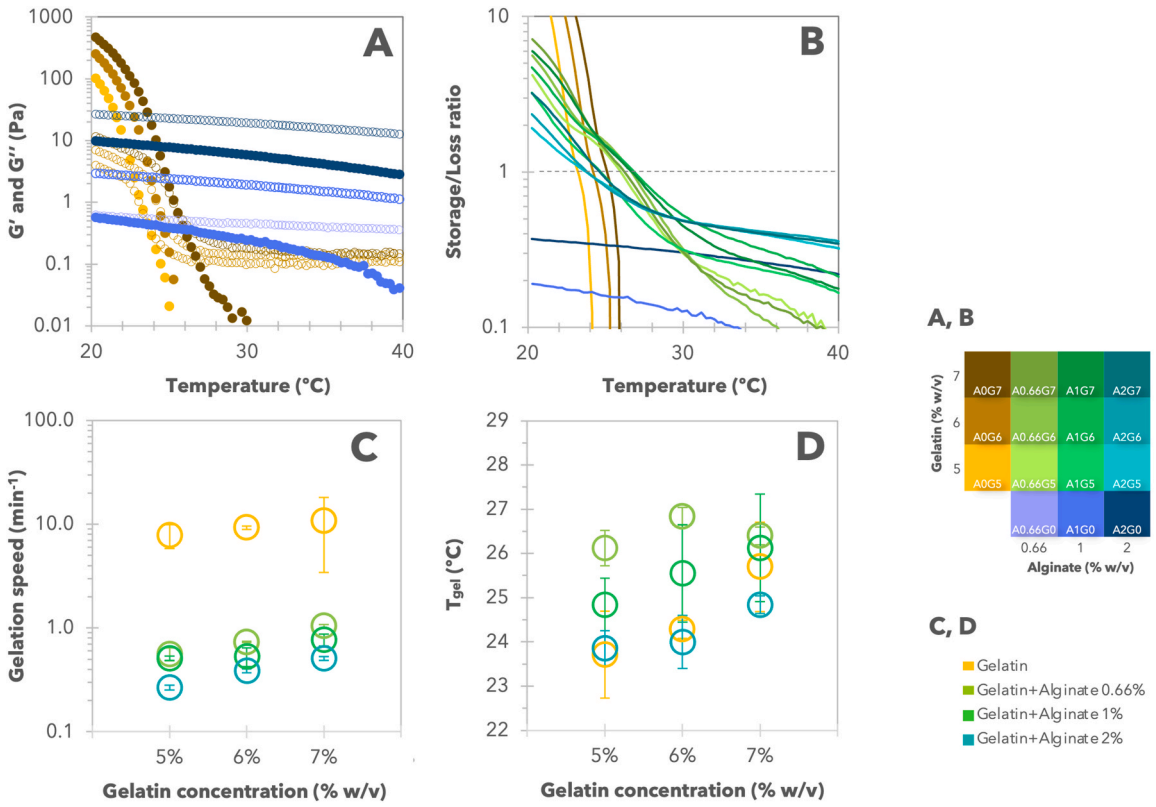

Fig. 2. A) T-ramps in oscillatory flow: Storage (G′) (solid circles) and Loss (G″) (empty circles) moduli of hydrogels of different concentrations of alginate or gelatin as a function of temperature performed at a constant frequency of 1 Hz and at a constant strain of 0.5% and a temperature change of −1 °C/min. B) Storage/loss ratio (G'/G″) as a function of temperature. The legend includes the color code followed for different bioink compositions. C) Gelation speed of the different mixtures studied, as calculated by the slope of Storage/loss respect to temperature (B). D) Gelation temperature (T_{gel}) of the different mixtures studied. Values represent Mean ± SD (n = 3).

2.3. Viscosity and shear thinning

During printing, bioinks experience high shear stress as they pass through a needle or nozzle, generating pressure that can compromise cell viability [20]. Therefore, materials that reduce viscosity under shear (shear-thinning behavior) are preferred. To evaluate this, viscosity flow curves were recorded between 0.1 and 1000 s^{-1} at 30 °C (above T_{gel}) and 20 °C (below T_{gel}), as shown in Figure S 3 A–B. The degree of shear thinning under these conditions is quantified in Fig. 3A and B. Statistical comparisons were performed using one-way ANOVA with Tukey's test (Supporting Information Table S 2, Table S 3).

As observed, viscosity increased with polymer concentration due to more supramolecular interactions. At 30 °C, gelatin contributed little to viscosity, while alginate and alginate-containing mixtures displayed higher viscosity and shear thinning. At 20 °C, gelatin strongly influenced viscosity, with shear-thinning values up to four orders of magnitude greater than alginate alone.

To further assess temperature effects, viscosity ramps from 20 to 30 °C were conducted (Figure S 3C), a range encompassing the T_{gel} of all gelatin-containing mixtures, and relevant for the printing process. Previous studies reported that gelation viscosity depends on gelatin concentration but not on temperature, while the role of alginate was not investigated [20]. In our results, viscosity increased with both gelatin and alginate concentrations. Alginate viscosity was temperature-independent, but gelatin viscosity rose by more than three orders of magnitude when cooled in this range. Consequently, mixtures also increased in viscosity when temperature decreased. Fig. 3C shows viscosity at 25 °C, near T_{gel}, where printing typically occurs. Both higher gelatin and alginate concentrations led to higher viscosity, consistent with earlier gelation at higher biopolymer content (Fig. 2 B). Significant

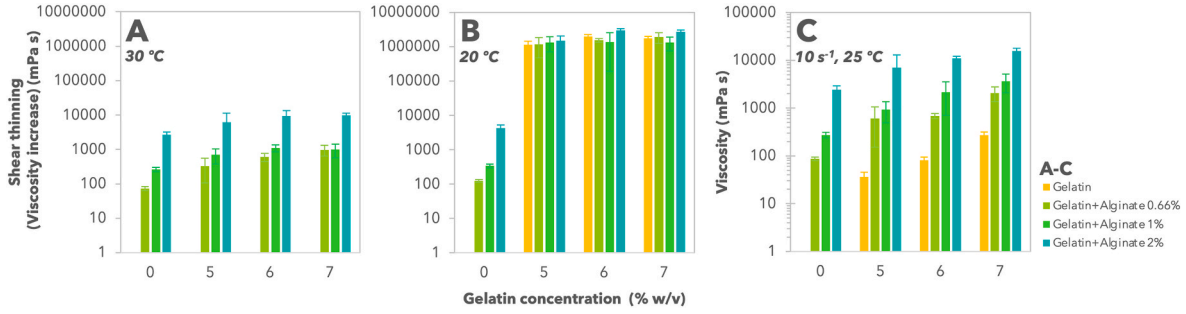

Fig. 3. A,B) Shear thinning (change in viscosity) in the range 0.1-1000 s^{-1} at 30 °C (A) and 20 °C (B). C) Viscosity of alginate, gelatin, or gelatin alginate solutions at 25 °C, close to the gelation temperature. Values represent Mean ± SD (n = 3). Significant differences ($P < 0.05$) were determined using one-way ANOVA with Tukey's multiple comparison tests (Supporting Information Table S 2-Table S 4).

differences ($P < 0.05$) were confirmed by ANOVA with Tukey's test (Supporting Information Table S 4).

Overall, these results indicate that alginate interactions are primarily concentration-dependent, whereas gelatin interactions are strongly temperature-dependent, due to changes in molecular kinetic energy. At 30 °C, gelatin molecules possess too much kinetic energy to interact; at 20 °C, reduced energy allows supramolecular interactions and network formation. In mixtures with alginate, the additional interactions created (hydrogen bonds and electrostatic forces) promote the network assembly even at higher temperatures (up to 40 °C). Among these, electrostatic interactions between alginate carboxylates and gelatin's amino (lysine), guanidine (arginine), and imidazole (histidine) groups likely play the dominant role, as they provide higher binding energies than hydrogen bonds [33,34]. This interpretation is consistent with spectroscopic evidence of alginate–gelatin interactions (FTIR, UV-vis) [35].

2.4. Printability screening

An ideal bioink must have adequate viscosity at low shear (before printing) to flow smoothly through the nozzle while preventing rapid cell sedimentation. At high shear (during extrusion), viscosity should decrease to minimize nozzle clogging and shear-induced cell death, but remain high enough to maintain material placement after deposition. Bioinks with shear-thinning behavior meet these requirements and can adapt to smaller nozzle diameters by compensating for higher shear. After deposition, the bioink should quickly increase its resistance to deformation and adopt solid-like behavior to stabilize the printed structure.

In alginate–gelatin bioinks, these requirements are achieved at different stages. Above T_{gel} (low shear), alginate provides sufficient viscosity and stabilizes the solution, making it less sensitive to temperature changes. At high shear (close to T_{gel}), both alginate and gelatin contribute to shear-thinning behavior. Below T_{gel} (resting state), gelatin network formation increases resistance to deformation and induces solid-like behavior, which is further enhanced by interactions with alginate.

Temperature plays a critical role in gelatin-containing mixtures and limits their printability. Bioprinters with precise printhead or print-bed temperature control are expensive, which restricts the use of gelatin despite its biocompatibility. For this reason, we assessed the printability of alginate–gelatin mixtures using a simpler bioprinter without temperature control (TissueStart®, TissueLabs). Bioinks containing alginate (1–2%) and gelatin (5–7%) were prepared at 37 °C (cell mixing temperature) and loaded into 5 mL syringes.

To efficiently assess a wide range of bioinks, both the CAD model and the printability evaluation strategy were optimized. A CAD design that can be printed rapidly while challenging three-dimensional shape fidelity is required for screening purposes. Accordingly, a cubic design ($5 \times 5 \times 5$ mm^3) was selected and printed repeatedly under varying printing temperatures and extrusion speeds. The syringe surface temperature, measured immediately before printing using a wireless infrared thermometer, was used as a proxy for the bioink temperature.

In parallel, we introduce the *Printability score* as a simple, semi-quantitative parameter for rapid assessment of printability. Several quantitative metrics have been previously described, including spreading ratio (fiber thickness relative to nozzle diameter) [36], the printability ratio (evaluating the squareness of a printed structure) [20], or the shape fidelity (evaluating the area of the pores of a grid) [37,38]. While robust, these approaches require image acquisition and analysis, which limits their efficiency when screening a large number of formulations and printing conditions.

For this reason, the *Printability score* was defined as a four-level scale ranging from 1 to 4. A score of 1 corresponds to liquid flow, resulting in an inability to stack layers; 2 corresponds to a viscous material capable of stacking multiple layers but producing poorly defined structures; 3 corresponds to a semisolid material capable of supporting all layers but with limited shape fidelity; and 4 corresponds to a semisolid or solid-like material that supports all layers and closely reproduces the CAD geometry. This approach enables rapid classification of bioink printability under defined temperature conditions without the need for quantitative image-based measurements. Bioinks identified as promising through this screening process were subsequently subjected to quantitative printability analysis using established metrics.

Table 2 shows the bioinks printed, printing conditions (printing temperature, difference between T_{gel} and printing temperature), viscoelastic parameters (T_{gel}, Storage/loss ratio, viscosity, shear stress, G'), and printability. Representative images of printed structures with 1% alginate and 5–7% gelatin are shown in Figure S 4.

Printability was strongly influenced by the composition and the printing parameters. Among the printing parameters, T_{print} had the greatest impact: printability improved as printing temperature approached T_{gel}. Scores of 3–4 were only achieved slightly below T_{gel}, when materials transitioned to solid-like behavior. However, if temperature dropped too far below T_{gel}, viscosity became too high and flow was hindered, reducing printability [8]. For instance, **A1G6** scored 4 at 25 °C (0.6 °C below T_{gel}) but dropped to 3 at 22 °C (3.6 °C below T_{gel}).

Since non-temperature-controlled printers are limited to room temperature, bioinks with higher T_{gel} broaden the printability window. In this case, lower alginate and higher gelatin concentrations favored this behavior. For example, **A1G5** showed a *printability score* 3–4 below 24 °C, while **A2G5** failed to reach good printability even at 23 °C. Similarly, higher gelatin content improved printability at higher temperatures, where **A1G6** and **A1G7** showed good printability below 25 °C, but **A1G5** only showed good printability below 24 °C.

Print speed also influenced outcomes. Optimal performance requires matching speed with gelation dynamics. At high viscosity and solid-like behavior, excessive print speed caused clogging and nozzle retention. Conversely, very low speeds prolonged printing, exposing bioinks to a wider temperature range and inconsistent behavior, although this might be noticeable in mixtures with rapid gelation (high gelatin, low alginate). For instance, **A1G7** printed between 25 and 23.5 °C scored 4 at 1 mm/s, but only 3 at 0.5 mm/s (poor definition of top layers) and 3 at 5 mm/s (poor definition from bottom to top).

2.5. Viscoelastic properties governing printability

Most studies to date have only used a limited number gelatin-alginate compositions under a controlled temperature and have focus on finding suitable printing parameters for a specific composition. Some of them, by looking for trends on the relationship between printing parameters. For instance, Q Li (2021), using a pressure-driven printer, found that a higher printing temperature requires either a lower printing pressure or a higher printing speed [21], but the effect of composition was not evaluated as only one mixture (gelatin 10%, alginate 2%) was studied.

Other studies found suitable printing parameters by looking for a relationship between the composition and the printing parameters. Ouyang et al. (2016) pointed that a higher gelatin concentration required higher printing temperature [20]; however, a limited number of temperatures (intervals of 2.5 °C) and gelatin concentrations (5, 7.5, and 10%) was tested, while the influence of alginate was not assessed. On the other hand, few authors attempted to correlate viscoelastic properties with printability using rheology. For example, Chung et al. [19] printed three gelatin-alginate mixtures at 5 °C and pointed the need of a solid-like behavior ($G' > G''$) for a good printability, whereas Paxton et al. [23] used only one gelatin-alginate composition at 37 °C and proposed rheological tests (yield stress, shear thinning, and recovery) to predict if a bioink could be printable. The most complete work is probably the one presented by Gao et al. [16], who printed 5 gelatin-alginate mixtures at 21 °C and found that the extrusion pressure needed depends on G' and G'' collectively, and proposed the loss factor (G''/G') as a viscoelastic property that permits predicting extrusion of

Table 2
Bioinks printed, printing parameters, and the resulting printability score. (a) Bioink's rheological properties gelation speed and T_{gel} as observed in Fig. 2. (b) Printing parameters: T_{print} is the printing temperature as measured in the surface of the syringe, Temp diff is the difference between T_{gel} and T_{print}. (c) Viscoelastic properties of the bioink at the corresponding printing temperature: viscosity, shear stress values (apparent rheological stresses from flow-curve measurements), G′, G″, and Storage/Loss ratio (G'/G"). (d) Printability score was assigned to each printed structure according to its fidelity with the CAD: A score of 1 corresponds to liquid flow, resulting in an inability to stack layers; 2 corresponds to a viscous material capable of stacking multiple layers but producing poorly defined structures; 3 corresponds to a semisolid material capable of supporting all layers but with limited shape fidelity; and 4 corresponds to a semisolid or solid-like material that supports all layers and closely reproduces the CAD geometry.

Bioink properties[a]			Printing parameters[b]			Viscoelastic properties[c]					Printability[d]
Bioink	Gelation speed (min^{-1})	T_{gel} (°C)	Print speed (mm/s)	T_{print} (°C)	Temp diff (°C)	Viscosity (mPa s)	Shear stress (Pa)	G′ (Pa)	G'' (Pa)	Storage/loss ratio[e]	*Printability score*
A1G5	0.51	24.9	4	30	5.2	501	5	1.7	5.6	0.29	1
A1G5	0.51	24.9	4	27	2.2	644	6	3.9	7.9	0.49	2
A1G5	0.51	24.9	4	26	1.2	749	7	6.5	9.7	0.61	2
A1G5	0.51	24.9	4	24.5	−0.4	1047	10	13.3	13.7	0.96	2
A1G5	0.51	24.9	4	24	−0.9	1223	12	15.4	15.0	1.03	3
A1G5	0.51	24.9	4	25	0.1	929	9	9.9	11.8	0.84	2
A1G5	0.51	24.9	4	24	−0.9	1223	12	15.4	15.0	1.03	3
A1G5	0.51	24.9	4	28.5	3.7	552	6	2.4	6.5	0.36	2
A1G5	0.51	24.9	4	27.5	2.7	608	6	3.1	7.3	0.43	2
A1G5	0.51	24.9	4	27	2.2	644	12	3.9	7.9	0.49	2
A1G5	0.51	24.9	4	27	2.2	644	12	3.9	7.9	0.49	3
A1G5	0.51	24.9	0.5	28	3.2	578	6	2.6	6.8	0.38	1
A1G5	0.51	24.9	0.5	27	2.2	644	12	3.9	7.9	0.49	1
A1G5	0.51	24.9	0.5	26.5	1.7	690	7	4.9	8.7	0.57	1
A1G5	0.51	24.9	0.5	25.5	0.6	830	8	7.4	10.3	0.72	1
A1G5	0.51	24.9	0.5	25	0.1	929	9	9.9	11.8	0.84	1
A1G5	0.51	24.9	0.5	24	−0.9	1223	12	15.4	15.0	1.03	2
A1G5	0.51	24.9	0.5	23	−1.9	2004	20	29.8	22.6	1.32	3
A1G6	0.53	25.6	5	25	−0.6	2123	21	16.8	15.4	1.09	4
A1G6	0.53	25.6	5	22	−3.6	17433	174	120.6	49.1	2.46	3
A1G6	0.53	25.6	5	22	−3.6	17433	174	120.6	49.1	2.46	3
A1G6	0.53	25.6	4	25	−0.6	2123	21	16.8	15.4	1.09	4
A1G7	0.77	26.1	0.5	27.5	1.4	1355	14	7.7	11.6	0.66	2
A1G7	0.77	26.1	0.5	25	−1.1	3626	36	33.9	26.2	1.30	3
A1G7	0.77	26.1	0.5	24.5	−1.6	5660	57	50.6	33.1	1.53	3
A1G7	0.77	26.1	5	23.5	−2.6	13616	136	95.3	46.3	2.06	3
A1G7	0.77	26.1	1	23.5	−2.6	13616	136	95.3	46.3	2.06	4
A1G7	0.77	26.1	1	25	−1.1	3626	36	33.9	26.2	1.30	4
A2G5	0.27	23.9	1	29	5.1	4659	47	22.1	41.6	0.53	1
A2G5	0.27	23.9	1	27	3.1	5492	55	32.1	49.4	0.65	1
A2G5	0.27	23.9	1	26	2.1	6134	61	39.6	54.2	0.73	1
A2G5	0.27	23.9	1	25	1.1	6981	70	54.0	62.8	0.86	1
A2G5	0.27	23.9	1	24	0.1	8678	87	69.9	71.8	0.97	2
A2G5	0.27	23.9	1	23	−0.9	12139	121	103.8	89.2	1.16	3
A2G6	0.39	24.0	1	28	4.0	7007	70	32.1	55.7	0.58	2
A2G6	0.39	24.0	1	26	2.0	8939	89	50.0	69.9	0.71	2
A2G6	0.39	24.0	1	24.5	0.5	12446	124	87.7	92.6	0.94	3
A2G6	0.39	24.0	1	23	−1.0	22368	224	160.7	125.7	1.28	3

continuous fibers, when the values range between 0.25 and 0.45. A list of relevant works on printability of gelatin-alginate mixtures is listed in Table 1.

These reports collectively indicate that lower printing temperatures require higher extrusion pressures or lower printing speeds, while higher biopolymer concentrations necessitate higher pressures or temperatures. However, these works considered very few gelatin-alginate mixtures and used temperature-controlled printers typically at one fixed temperature. A comprehensive understanding of how gelatin and alginate concentrations, together with temperature, influence viscoelastic properties—and how those properties govern printability—enables predictive tailoring of bioinks and their printing conditions.

In this work, we systematically explored a much broader compositional and thermal space (0.66–2 % alginate, 5–7 % gelatin) and link four parameters —viscosity, Storage/loss ratio, T_{gel}, and printing speed—to printability. Table 2 permits identifying viscosity and Storage/loss ratio as the two viscoelastic properties required for good printability regardless of the composition. T_{gel}, on the other hand, defines the operational window, allowing the identification of the ideal printing temperature range over which the bioink meets such rheological conditions. The printing speed is then tuned based on viscosity to ensure continuous filament flow.

Fig. 4 illustrates the relationship between viscosity, Storage/loss ratio, printing speed, and printability. A *printability score* of 4 was achieved only when viscosity was between 2123 and 13616 mPa s and Storage/loss ratio was between 1.0 and 2.1. These conditions are typically met when the printing temperature ranges between 0.6 and 2.6 °C below T_{gel}. Although the loss factor window proposed by Gao et al. [16] points the need of a solid-like behavior (loss factor of 0.25 to 0.45, equivalent to Storage/loss ratios between 2.2 and 4), our findings show that lower values, immediately upon reaching a solid-like behavior (1-2.1), result in better defined filaments and sufficient resistance to deformation to prevent layer fusion and hold several layers on top of each other.

Subsequently, printing speed should be tuned based on viscosity to guarantee continuous flow. For example, mixtures such as **A2G5**, with higher alginate and lower gelatin, exhibited high viscosity at the printing temperature (Fig. 3C) and so they required low printing speeds to avoid incomplete deposition. In contrast, **A1G6** (lower alginate, higher gelatin) printed successfully at higher speeds due to lower viscosity. Fig. 4 (D) shows a 3D scatter plot of the viscosity, Storage/loss ratio, and printing speed, and their influence on the *printability score* (indicated by circle size).

Extrapolation of these relationships for a given bioink composition

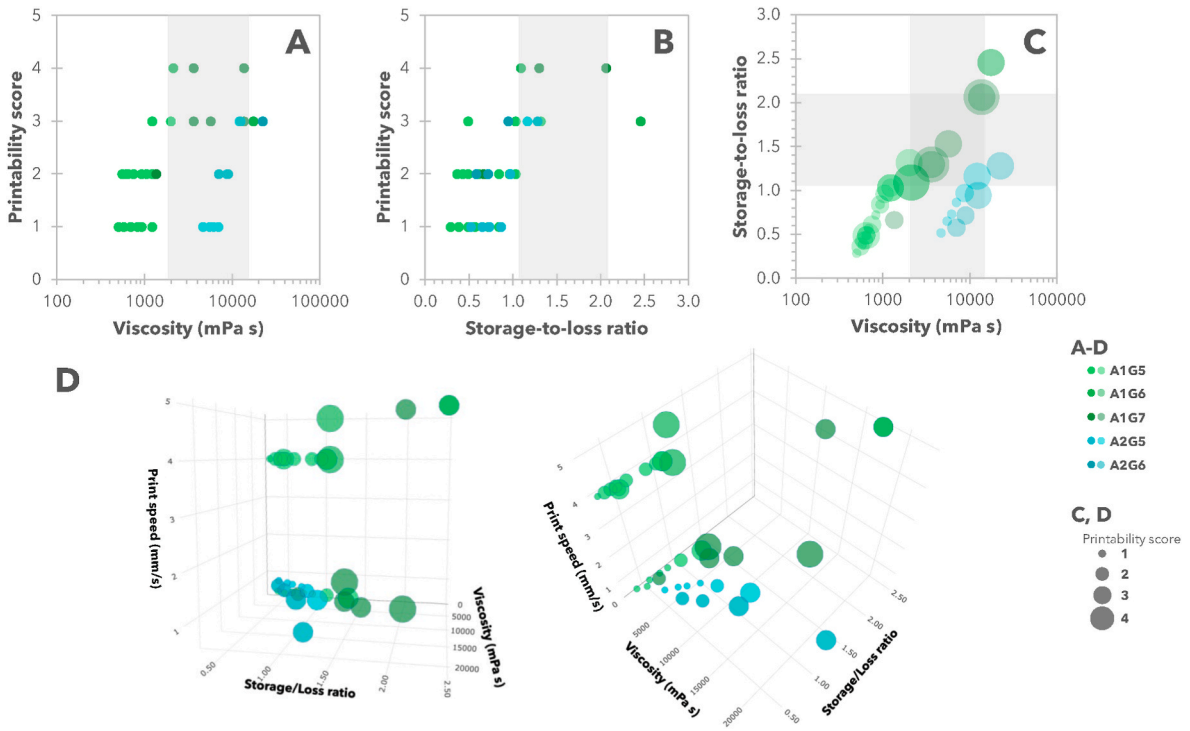

Fig. 4. Correlation of viscoelastic properties and printability. (A) Printability score as a function of viscosity. (B) Printability score as a function of Storage/loss ratio. (C) Printability score circle size) as a function of Storage/loss ratio and viscosity. Gray rectangles indicate the suitable ranges for good printability. (D) 3D scatter plot showing printability score (circle size) as a function of Storage/loss ratio, viscosity, and print speed.

enables prediction of the temperature ranges over which the required viscoelastic properties are satisfied. Fig. 5A–D presents three-dimensional plots of temperature, viscosity, and storage-to-loss modulus ratio (G'/G'') across bioink compositions, where parallel planes delineate the viscoelastic window associated with successful printability.

In bioprinters lacking active temperature control, the bioink temperature at any given time point depends on its initial temperature, the ambient room temperature, and the cooling rate of the bioink. The printing time window can therefore be obtained from the cooling kinetics at room temperature, where the bioink transits in and out of the temperature (and viscoelastic) window at predictable times, allowing scheduled printing. Bioinks were initially equilibrated at 37 °C, corresponding to cell-mixing conditions, and subsequently exposed to a constant room temperature while continuously recording the bioink temperature (Fig. 5 E). All bioinks exhibited cooling behavior well described by a one-phase exponential decay model, with cooling rates depending on the composition. The corresponding regression parameters are provided in the Supporting Information (Table S4).

Based on this analysis, Table 3 identifies the formulations with favorable viscoelastic properties for good printability and their corresponding temperature windows, showing that **A1G6** and **A1G7** exhibit the broadest temperature ranges (2.4 °C and 2.0 °C, respectively). Correspondingly, **A1G6** and **A1G7** showed the broadest printing time ranges (14.1 and 7.2 min, respectively). Although the cooling kinetics will follow the same one-phase behavior at different ambient temperatures, the cooling rate is temperature dependent for which it should be calibrated at any different room temperature to obtain an accurate time window.

2.6. Validation of the predicted window

The predicted printability temperature windows (Table 3) were first validated by three parameters which assess printability in the horizontal plane: spreading ratio, shape fidelity, and printability ratio. The spreading ratio was determined by printing single filaments in a 20×20 mm^2 mesh (Fig. 6 A) and calculating filament thickness relative to the CAD design. Values > 1 indicated spreading due to excessive flow. Results for each composition are shown in Fig. 7A–E. Shape fidelity and printability ratio were assessed by printing quadrangular prisms ($10 \times 10 \times 2.52$ mm^3) (Fig. 6 B). Shape fidelity, shown in Fig. 7F–J, was calculated as the printed area relative to the CAD design, with values > 1 indicating expansion due to spreading. Printability ratio, shown in Fig. 7K–O, describes squareness: values < 1 indicate rounded edges caused by flow, while values > 1 indicate over-gelation.

All three parameters were strongly influenced by temperature, with values approaching 1 as bioink temperature decreased towards the predicted range. Spreading ratio deviated the most from 1, reflecting the difficulty of maintaining resolution in single-filament structures. Increasing gelatin content (with lower alginate) led to faster gelation, raising viscosity and Storage/loss ratio as temperature dropped, thereby reducing spreading (Fig. 7C–E). Conversely, higher alginate content stabilized viscosity, producing more consistent spreading ratios across temperatures (Fig. 7A and B). Variability at high polymer concentrations (A, D, E) reflected irregular filaments (Fig. 6: **A2G5**, **A1G7**, A0.**66G7**), consistent with their higher resistance to flow. Lower polymer concentrations (B, C) yielded straighter, more homogeneous filaments due to lower viscosity.

In larger structures, both shape fidelity and printability ratio remained close to 1 within the predicted printability ranges, confirming the predictive value of viscoelastic properties. Printability ratio values stayed between 0.8 and 1 across all compositions, with similar slopes, indicating that sharp corners could be printed consistently. Shape fidelity values approached 1 as the temperature neared the predicted range, though differences in slope (Fig. 7F–J) highlighted a stronger dependence on composition. Higher alginate content with lower gelatin resulted in constructs larger than the CAD model at higher temperatures, as indicated by higher shape fidelity values.

Next, the vertical accuracy was also assessed as differences with the CAD model can become more evident in multi-layered structures. For

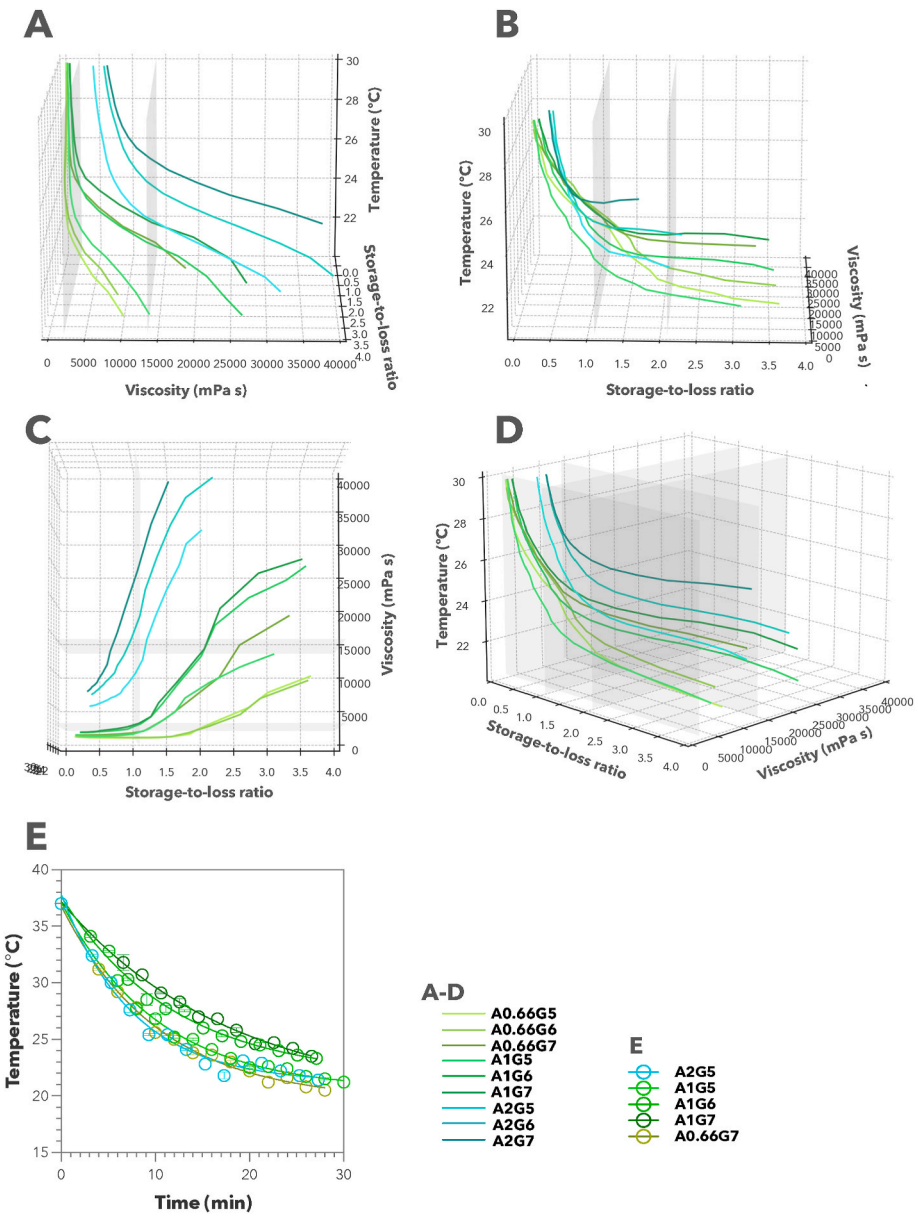

Fig. 5. (A-D) 3D scatter plot showing the relationship between viscosity, Storage/loss ratio, and temperature. Parallel planes in the viscosity and Storage/loss ratio indicate the suitable ranges for good printability. (E) Cooling kinetics of bioinks with predicted printability when exposed to a constant room temperature (19.6 ± 0.2 °C).

Table 3
Temperature-dependent viscoelastic properties (Storage/loss ratio and viscosity at 10 s^{-1}) defining printability of gelatin-alginate bioinks and their corresponding temperature window. a) A practical room-temperature time window derives from the cooling kinetics of bioinks at a constant room temperature (19.6 ± 0.2 °C). b) Shear stress of bioink within the printability window (apparent rheological stresses from flow-curve measurements).

Bioink	Storage/loss [1.0 – 2.1]	Viscosity [2123 - 13616] (mPa s)	Temperature window (°C)	Temperature range (°C)	Time window[a] (min)	Time range (min)	Shear stress[b] (Pa)
A0.66G7	1.5 – 1.8	3385 – 5839	24.1 – 24.6	0.5	12.7 - 13.8	1.1	33.8 – 58.4
A1G5	1.4 – 1.8	3050 – 6799	21.7 - 22.7	1	20.5 – 26.6	6.1	30.5 – 68.0
A1G6	1.0 – 2.0	2123 – 12726	22.7 – 25.1	2.4	18.3 – 32.4	14.1	21.2 – 127.3
A1G7	1.1 – 2.1	2596 – 13616	23.6 – 25.6	2	19.1 – 26.3	7.2	26.0 – 136.1
A2G5	1.1 - 1.2	10102 - 12139	23.2 – 23.6	0.4	14.7 - 16.1	1.4	101.0 – 121.4

this, quadrangular prisms of 10 x 10 × 5 mm^3 (12-layered structures) were printed with each bioink within their predicted temperature windows and are shown in the Supporting Information (Figure S 5). The height of the structures was measured immediately after printing (Fig. 8 A). Hight accuracy measurements showed values ranging from 110.7 + 1% using **A1G5**, to 117.0 + 0.6% using **A1G7**, indicating a lower printing fidelity in the vertical plane than in the horizontal plane. Among different bioink compositions, a slight tendency is observed where a higher total polymer concentration results in taller structures, although no significant differences were found across compositions

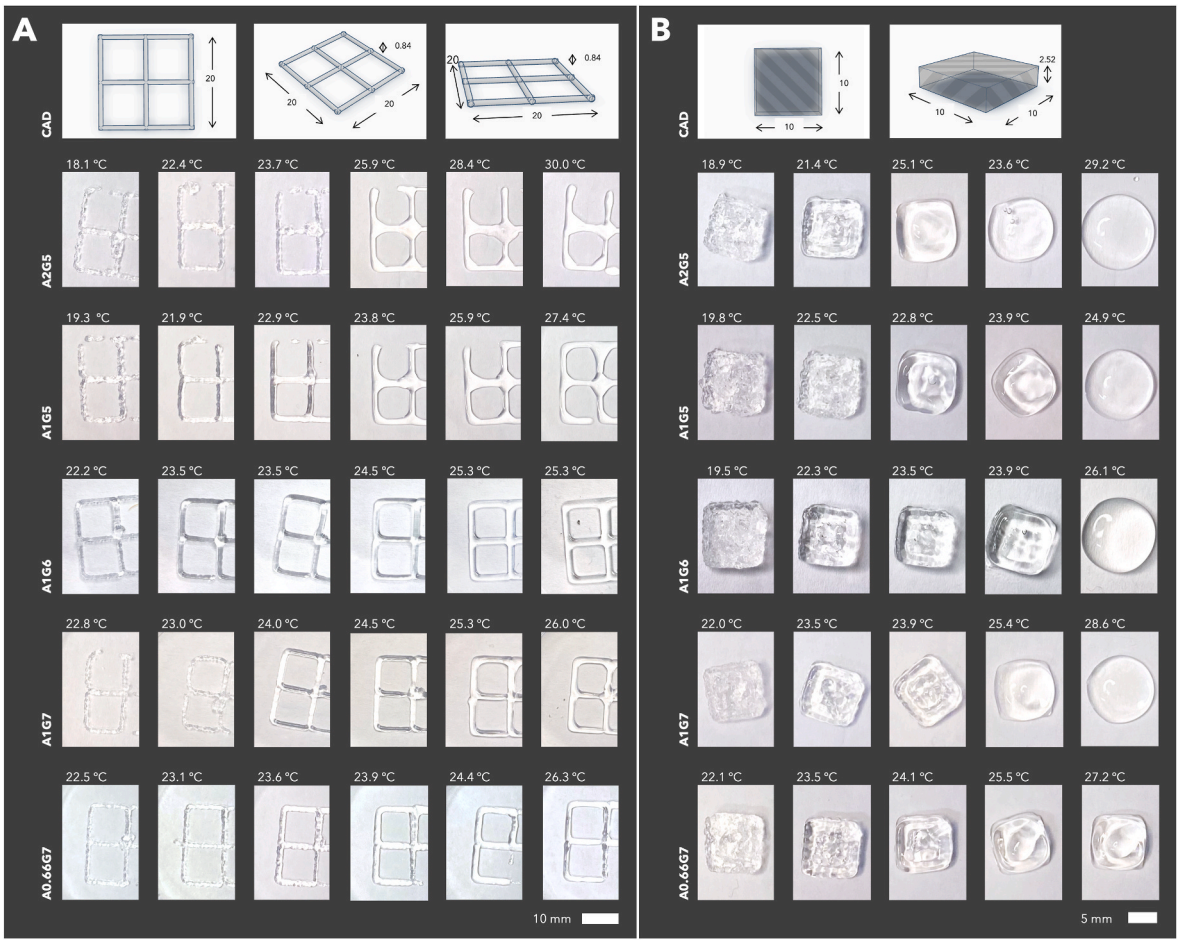

Fig. 6. (A) CAD of single-filament mesh structure designed including its measurements (mm) (top) and printed with different bioink compositions at different temperatures (°C) for the estimation of the spreading ratio. Scalebar represents 10 mm and is equivalent for all images. (B) CAD of quadrangular prism designed with its measurements (top) and printed (bottom) using different bioink compositions at different temperatures (°C) for the determination of the shape fidelity and the printability ratio. Scale bar represents 5 mm and is equivalent for all images.

($p > 0.05$). Moreover, as 3D structures can undergo creep upon printing, a time-dependent deformation because of their own weight, the height stability of these multi-layered structures was assessed over time. Fig. 8 B shows that the height of the structures remains highly stable ($p > 0.05$) for at least 60 min after printing, allowing for sufficient time between the printing and the crosslinking process. Pictures of printed prisms over time (Figure S 5) and statistical analyses (Table S 5) can be found in the Supporting Information.

The printability of more complex structures and containing different bioinks was demonstrated by a composite 10 x 10 × 10 mm^3 prism with bioink **A1G6**, containing a 2 × 10 mm horizontal cylinder in the middle printed with **A1G5**. This was performed in a 3-step subsequent printing process: (1) bottom, (2) cylinder, and (3) top, where the corresponding bioinks were extruded within their predicted printability window (Fig. 9). The staining of **A1G5** with trypan blue at 0.4% permitted the visualization of the composite structure with defined shapes, where the embedded cylinder has a diameter of 1.96 ± 0.19 mm (printing accuracy of 98.1 ± 9.5%).

2.7. Stability under incubation

The effectiveness of the crosslinking process for maintaining stable constructs under culture conditions (DMEM:L-15, 37 °C, 5% CO_2) was evaluated by monitoring the diameter and height of printed structures after 1, 3, 7, and 14 days of incubation. Fig. 10 A shows CAD designs and printed constructs from **A1G6** and **A1G7** bioinks before and after incubation, while Fig. 10 B presents the degradation profiles. Both formulations allowed rapid and homogeneous diffusion of culture medium, as indicated by the uniform pink coloration from day 1, and remained stable for at least 14 days. Diameter values showed no significant degradation for either formulation throughout the incubation period ($P > 0.05$). In terms of height, **A1G6** decreased to 65.1 ± 14.3% at day 3 ($P < 0.05$) but partially recovered to 76.4 ± 6.8% by day 14. **A1G7** showed a non-significant reduction to 72.4 ± 9.8% ($P > 0.05$) with recovery to 85.6 ± 4.6% by day 14. These observations suggest a balance of slow degradation and swelling, resulting in overall structural stability over two weeks. Statistical analyses (one-way ANOVA with Tukey's test) are provided in Supporting Information (Table S 6 and Table S 7).

Together, these results confirm that the crosslinked alginate–gelatin constructs retain their shape and dimensions under physiological culture conditions, supporting their potential for tissue engineering applications.

2.8. Biocompatibility

To determine whether gelatin–alginate hydrogels can support viable cells, the biocompatibility of the **A1G7** formulation was evaluated using MDA-MB231 triple-negative breast cancer cells. Bioink **A1G7. MDAMB231** was prepared by suspending cells at 1.9 × 10^6 cells/mL in the hydrogel. Aliquots of 100 μL were extruded into 96 well plates; after 1 min to allow partial solidification, constructs were crosslinked in a calcium bath, rinsed with PBS, and incubated in L 15 medium at 37 °C.

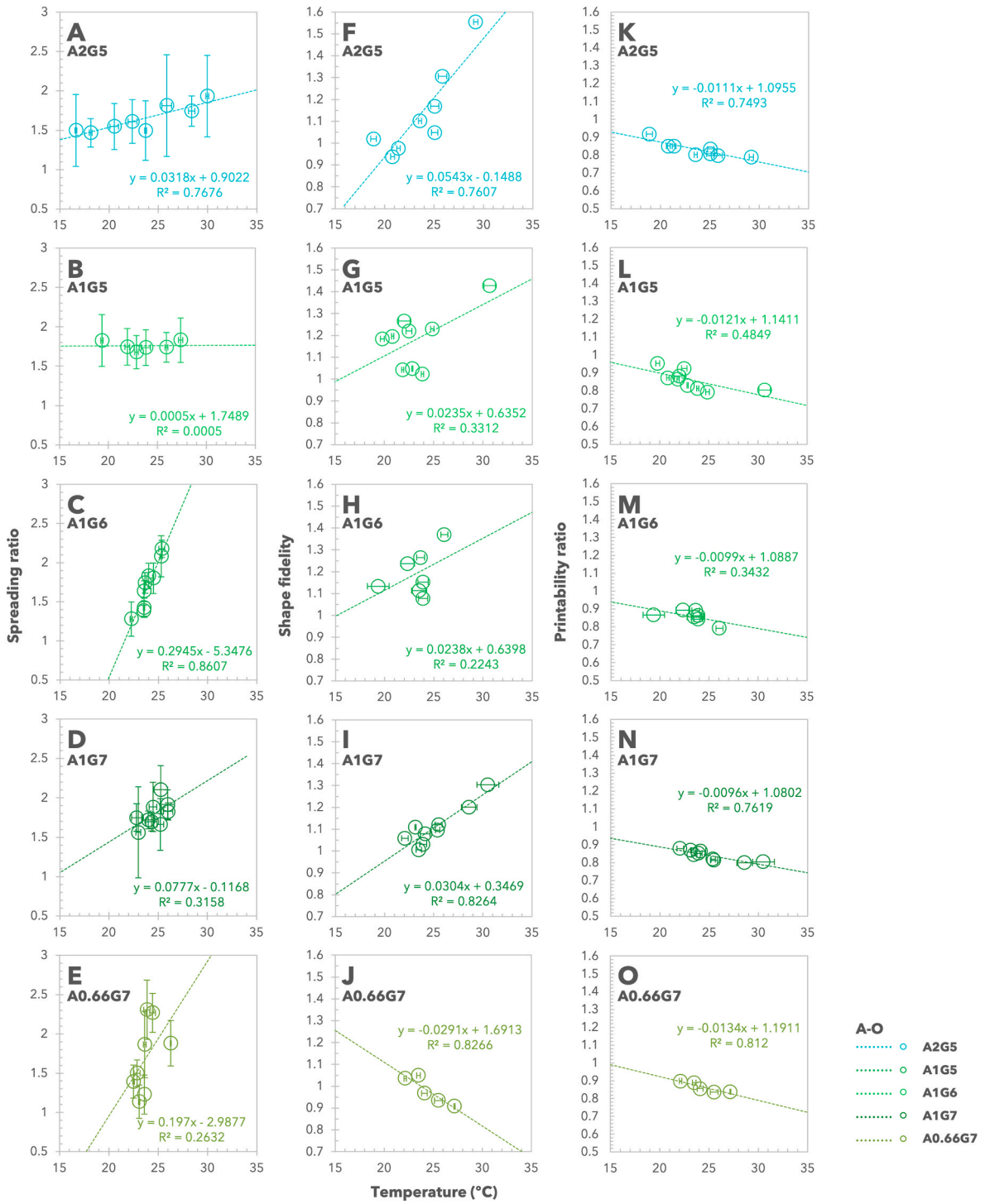

Fig. 7. (A-E) Spreading ratio of printed single filaments as a function of temperature (thickness relative to the CAD design). Values are Mean ± SD (n ≥ 4). (F-J) Shape fidelity as a function of temperature (printed area relative to CAD design). (K-O) Printability ratio as a function of temperature (squareness of printed structures). Error bars on X-axis represent temperature variation during printing (SD, n ≥ 4).

Live/dead staining followed by confocal fluorescence microscopy allowed visualization and quantification of viable and non-viable cells. Representative micrographs are shown in Fig. 11 A with viability results in Fig. 11 B. MDA-MB231 cells exhibited high viability within the **A1G7** hydrogel: 96.0 ± 2.4 % after one day and 82.7 ± 5.3 % after nine days. The low variation underscores the reproducibility of the measurements and the suitability of confocal microscopy for three-dimensional constructs.

Differences in cell morphology were observed between 2D and 3D conditions: on rigid two-dimensional surfaces cells spread and flatten, whereas within the hydrogel they remained rounded due to uniform mechanical forces around them. Shie et al. previously reported that cells encapsulated in methacrylated gelatin adopt rounder morphologies and proliferate more slowly at higher polymer concentrations, reflecting increased stiffness [39]. Overall, these results confirm that gelatin–alginate hydrogels are biocompatible and support the growth of cancer cells over extended culture periods.

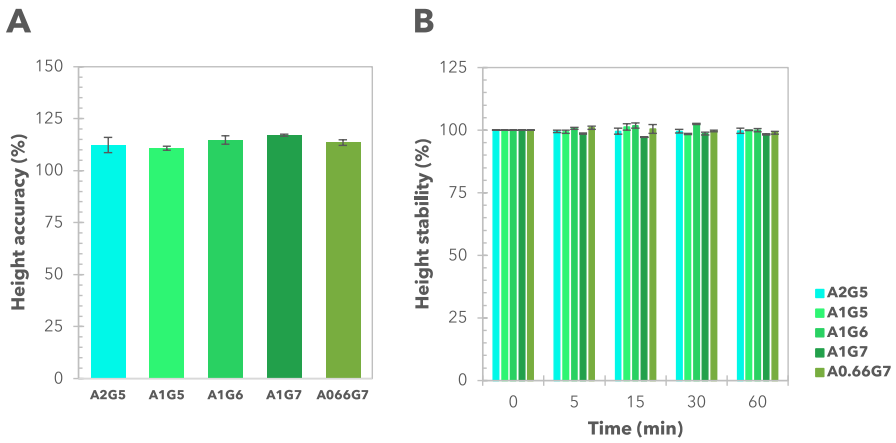

Fig. 8. A) Hight accuracy of structures printed with different bioinks. (B) Height stability along time of structures printed with different bioinks.

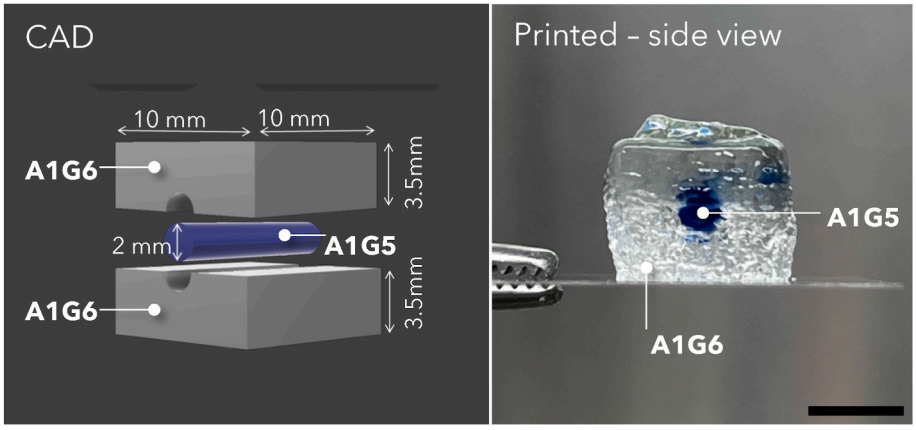

Fig. 9. Composite structure (prism containing a cylinder) fabricated in a 3-stage subsequent printing process with two bioinks. Scalebar represents 5 mm.

2.9. Influence of the printing process on cell viability

To assess whether the shear forces during extrusion compromise cell survival, we printed the **A1G7.MDAMB231** bioink under the optimized conditions identified previously. The printer was sterilized (70 % ethanol) and operated within a laminar-flow hood. Bioink containing MDA-MB-231 cells (8×10^6 cells/mL) was extruded at 25 °C using the same needle diameter and print speed as in the printability tests. After crosslinking, constructs were incubated for 24 h, stained using a live/dead assay, and imaged by confocal fluorescence microscopy (Fig. 12).

A uniform suspension of cells was observed throughout the printed constructs, similar to the lower cell density used in biocompatibility experiments, indicating the preparation protocol is robust across cell densities. The higher cell density resulted in closer proximity of cells, showing that cell concentration can be tuned to achieve desired tissue density. Cells were present right up to the construct edges, demonstrating that gelatin–alginate bioinks can produce live tissues with micrometre scale resolution.

Previous studies have shown that printing pressure and nozzle diameter can influence cell survival [28]; biopolymer concentration also affects viability [24]. Shear stress—the product of viscosity and shear rate—has been reported to correlate exponentially with viability, with 100 Pa reducing survival to around 80 % [20]. In our conditions, MDA-MB-231 viability remained high: 92.4 ± 2.2 % after 1 d and 96.5 ± 0.9 % after 8 d, comparable to the biocompatibility experiments. These results indicate that the printing process, including cooling the bioink to ~25 °C and the corresponding shear stress at this temperature, does not adversely affect cell viability. Table 2 shows the apparent shear stress of the bioink at a given temperature, extracted from rheological studies (viscosity vs. temperature) at a constant shear rate of 10^{-1}, resembling extrusion through the needle, which were generally below 100 Pa. A direct calculation of the shear stressed experienced by cells using an accurate shear rate based on the nozzle diameter and extrusion flow, however, would provide more accurate results and is envisaged for future studies.

3. Conclusions

This work establishes a predictive, temperature-aware framework for optimizing thermosensitive gelatin–alginate bioinks that can be printed without active thermal control. We identify a printability window defined by viscosities of 2123–13,616 mPa s and a storage/loss ratio (G'/G'') of 1.0–2.1, typically attained at printing temperatures 0.6–2.6 °C below Tg_{el}. Together with the room-temperature printing-time window derived from cooling/gelation kinetics, these quantitative bounds enable operators to plan when to print and what rheological targets to meet on low-cost systems.

Unlike prior studies that emphasize single compositions or qualitative descriptors, our systematic exploration across multiple gelatin-alginate formulations shows that viscosity and the Storage/loss ratio (G'/G'') are the primary rheological predictors linked to extrusion continuity, geometric fidelity, and multilayer stability. In contrast, gelation temperature and gelation kinetics act as operational schedulers, defining the temperature and time interval over which those optimal rheological conditions are met. This distinction converts rheological data into actionable design targets for bioink formulation and process timing.

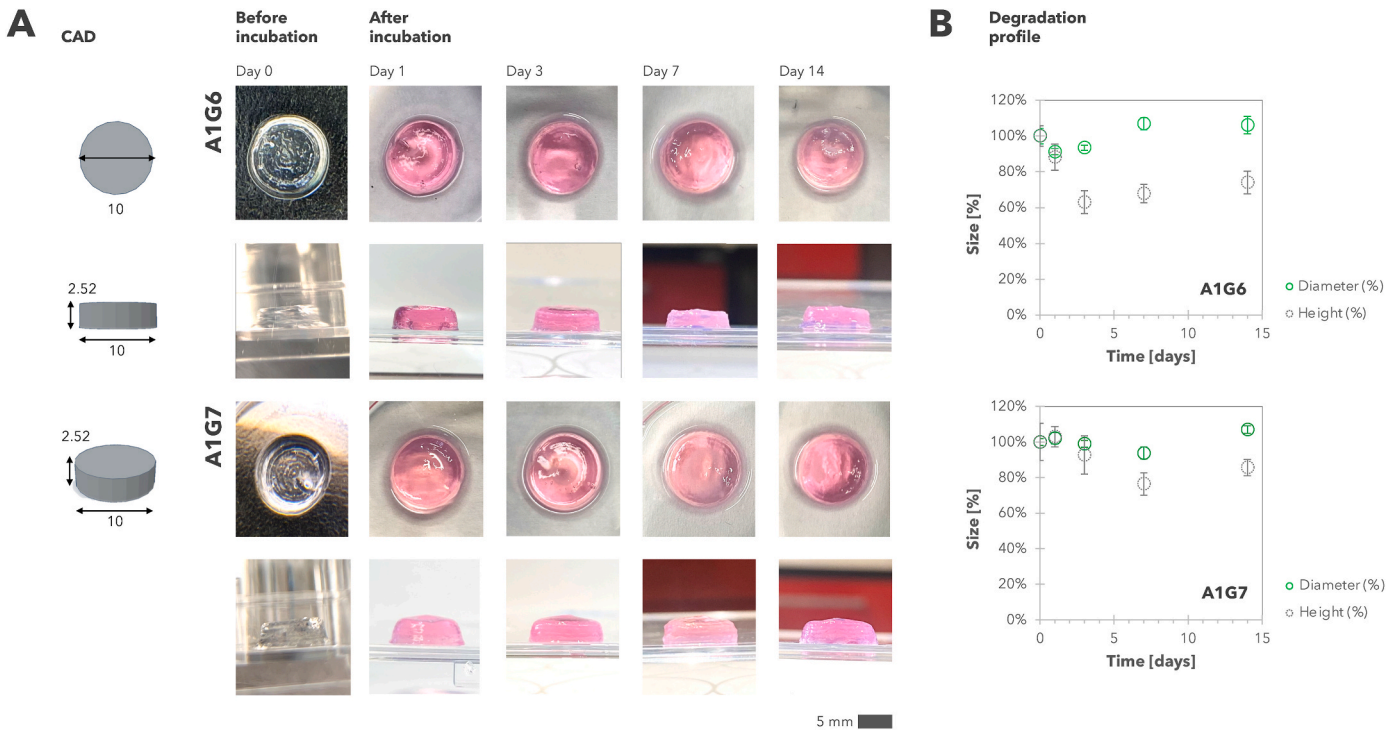

Fig. 10. (A) CAD (cylinder 10 × 2.52 mm) and printed structures using bioinks **A1G6** and **A1G7** before and after incubation for different times under cell culture conditions (DMEM:L-15 1:1 culture media, 37 °C, 5% CO_2). Scale bar represents 5 mm and is equivalent for all images. (B) Degradation profile (diameter and height) of printed structures under culture conditions. Significant differences ($P < 0.05$) were determined through one-way ANOVA with Tukey's multiple comparison tests (Supporting Information Table S 6 and Table S 7).

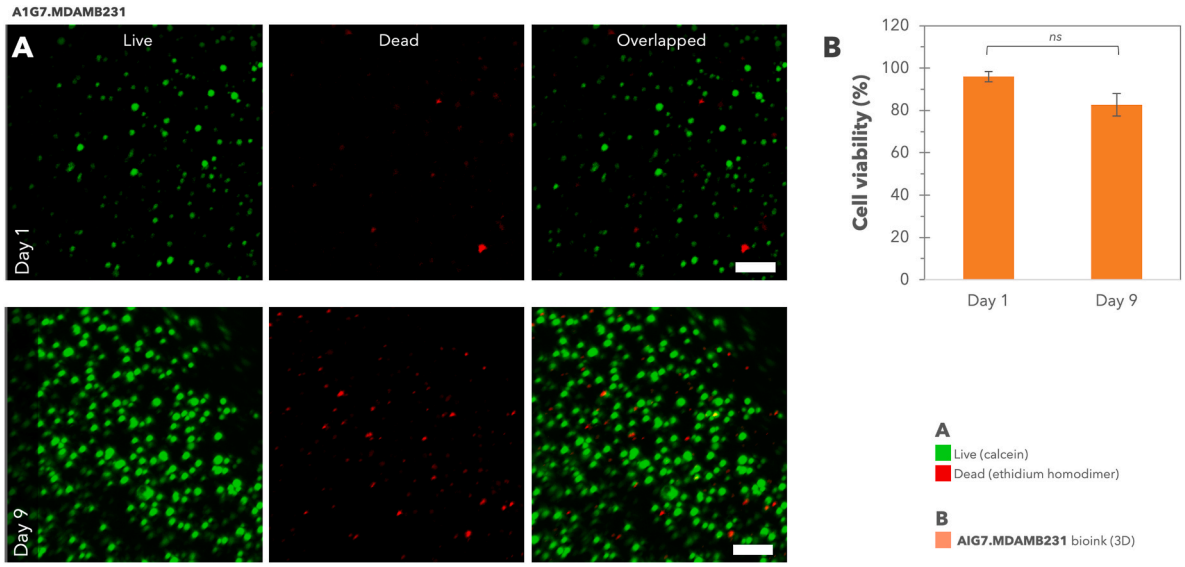

Fig. 11. (A) Confocal fluorescence microscopy images of bioink **A1G7.MDAMB231** after 1 (top) or 9 (bottom) days incubation. Green: calcein (live); red: ethidium homodimer (dead). Scale bar represents 100 μm and is equivalent for all images. (B) Cell viability of bioink **A1G7.MDAMB231** after 1 or 9 days incubation as calculated by live/dead staining under confocal fluorescence microscopy. Values represent Mean ± SD (n = 3). ns: no significant differences ($P < 0.05$) were found.

We validate the framework by quantitative printability parameters such as spreading ratio, shape fidelity, printability ratio, and height fidelity, demonstrating multilayer stability (12-layer prisms with height-retention maintained over 60 min) and by fabricating a composite construct (a prism containing an internal cylinder printed in three stages, 17 layers, 7 mm total height). Under these predicted conditions, constructs supported high viability of MDA-MB-231 cells (92–96% over nine days), consistent with operation within the identified rheological window.

By reducing reliance on costly temperature-controlled hardware, this methodology broadens access to 3D bioprinting, particularly in resource-limited settings, and facilitates the fabrication of biologically relevant cancer models. Future work will extend this framework to additional cell types and thermosensitive polymers, incorporate direct force/pressure sensing to complement rheology-based estimates, and address more complex tissue architectures to further expand

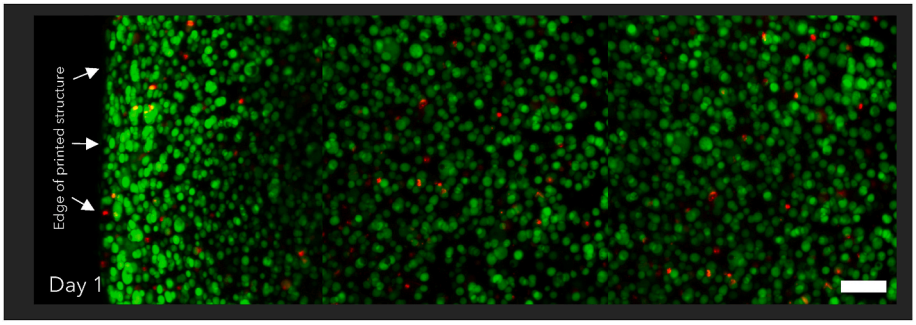

Fig. 12. Stitched confocal fluorescence microscopy Z-projections of bioink **A1G7.MDAMB231** after 1-day incubation. Green: calcein (live); red: ethidium homodimer (dead). The cells are homogeneously distributed across the structure upon printing, including on the edges (A, left side), evidencing the suitability of gelatin-alginate bioinks for the construction of live tissues with micron-scale resolution. Scale bar represents 100 μm.

applicability in tissue engineering and disease modeling.

4. Materials and methods

4.1. General methods

Rheology: The rheological characterization of alginate and gelatin mixtures was performed with a Modular Compact Rheometer MCR 502 (Anton Paar, Madrid, Spain), equipped with an electric plate for temperature control (±0.01 °C). A parallel-plate geometry, with a diameter of 50 mm and a gap of 1.0 mm was used.

The gel transition was evaluated through a temperature ramp test, where the G′ and G″ behaviour was evaluated in the range of 40 to 20 °C, with temperature rate of 1 °C/min, at a constant frequency of 1 Hz and imposing a 0.5% strain (within the linear viscoelastic regime, LVR).

Steady-shear flow measurements were performed to characterize the apparent viscosity flow curve in the shear rate range of 0.1 to 1000 1/s, at 20 and 30 °C. The viscosity was also measured at a constant shear-rate value of 10 1/s imposing a temperature ramp in the range of 30 to 20 °C, with a temperature rate of 1 °C/min.

Brightfield and fluorescence microscopy: a Nikon eclipse TiS research microscope equipped with epi-fluorescence illuminators and fluorescence filters was used.

Confocal fluorescence microscopy: a Zeiss LSM 700 Confocal laser microscope equipped with Z drive step motor, reflected-light objective lenses, and laser lines at 488 and 555 nm wavelength was used.

4.2. Preparation of hydrogels and solutions

Hydrogels: The corresponding amount of Gelatin from porcine skin (Type A, gel strength 300, Sigma-Aldrich, G2500-100G) and sodium alginate (AppliChem, A3249) powders was weighed in a precision scale, added to PBS (Sigma-Aldrich) at 75 °C, and left under magnetic stirring at 75 °C for 2 h. The concentration of polymers is always expressed as % w/v. The resulting hydrogel was centrifuged at 2000 rpm for 5 min to remove air bubbles and subsequently stored at 4 °C and used within 72 h.

For biological experiments, alginate and gelatin powders were sterilized via UV exposure in CL-1000 Ultraviolet Crosslinker (UVP) for 120 min and the preparation was carried out under sterile conditions inside a laminar flow hood.

Live/dead staining solution was composed of 0.2 μL/mL calcein (Biotium), 0.8 μL/mL ethidium bromide (Biotium), and 25 μL/mL 4-(2-hydroxyethyl)-1-piperazineethanesulfonic acid buffer solution (HEPES, 1M in H2O; Sigma-Aldrich) in DMEM culture medium.

4.3. Solubility and manual extrusion

Solutions at different concentrations of alginate (0.1 – 10%), gelatin (0.1 – 10%), or mixtures of both (as shown in) were prepared by adding the corresponding amount of each biopolymer to 10 mL PBS at 75 °C and were set under magnetic stirring at the same temperature. After one and 2 h, complete solubilization was verified. Biopolymer solutions were loaded into 5 mL syringes and were left to cool down. Temperature was measured in the outer part of the syringe using a wireless infrared thermometer. A sample of the solution was extruded manually when the temperature was 35, 30, 25, or 20 °C onto petri dishes, while the pressure for extruding as well as the consistency of the extruded material was assessed. After extrusion, the mixtures of gelatin alginate were immersed in a 100 mM CaCl2 solution for 1 min, after which they were washed with deionized water. Samples were examined for changes in consistency and morphology.

4.4. Gelation and strength

Hydrogels of alginate (0.66, 1, and 2 % w/v), gelatin (4, 5, and 6%), and the corresponding mixtures of both biopolymers were loaded onto the rheometer using a 50 mm plate-plate geometry. For each gel, temperature ramps from 40 to 20 °C were performed at a constant frequency of 1 Hz and at a constant strain of 0.5% (within the linear viscoelastic region) and a temperature change of −1 °C/min and the Storage (G′) and Loss (G″) moduli were determined. The gelation temperature T_{gel} was defined for each gel as the temperature where G' = G''.

4.5. Viscosity

The shear thinning behavior was studied for each gel by performing viscosity ramps at a constant temperature (30 °C and 20 °C) by decreasing the shear rate from 1000 to 0.1 s^{-1}. The shear thinning for each hydrogel was determined at both temperatures as the difference between viscosities at 0.1 and 1000 s^{-1}.

The influence of temperature on the viscosity of the mixtures was studied by performing viscosity T-ramps in the range of 20 - 30 °C (between which the T_{gel} of all gelatin-containing mixtures is observed), at a constant shear rate of 10s^{-1}.

Significant differences ($P < 0.05$) were determined by performing a one-way ANOVA with Tukey's multiple comparison tests were performed using Python.

4.6. Printability screening

Gelatin alginate mixtures (as indicated in Table 2) were loaded into 5 mL syringes when being at ~40 °C. A 18G needle (0.838 mm nominal internal diameter) was connected to the syringe and loaded into a TissueStart ® (Tissuelabs) bioprinter. Calibration procedure was performed according to the manufacturer's instructions. Printing temperature (T_{print}) was determined by measuring the temperature of the outer part of the syringe using a wireless infrared thermometer. Disposable Petri

dishes were placed over the print bed (or metallic structure) to print the structures. A cubic 5x5x5 mm^3 CAD design was subsequently printed while the temperatures were monitored at the time of printing. The print speed was adjusted as indicated in Table 2. The printability was assessed by means of the *printability score* relative to the CAD design, defined as a four-level scale ranging from 1 to 4. A score of 1 corresponds to liquid flow, resulting in an inability to stack layers; 2 corresponds to a viscous material capable of stacking multiple layers but producing poorly defined structures; 3 corresponds to a semisolid material capable of supporting all layers but with limited shape fidelity; and 4 corresponds to a semisolid or solid-like material that supports all layers and closely reproduces the CAD geometry.

4.7. Viscoelastic properties governing printability

Results from rheology experiments were analyzed and plotted using Microsoft Excel. 3D-scatter plots were performed using Plotly, implemented either in R or Python.

The printability viscoelastic window was defined as the range of viscosity and Storage/loss modulus ratio for which printed structures achieved a *printability score* of 4, independent of bioink formulation. This window corresponded to viscosities between 2123 and 13616 mPa s, and Storage/loss ratio between 1.0 and 2.1).

The predicted printing temperature window for each bioink was defined as the temperature window where the bioink complies with the printability viscoelastic window.

4.8. Bioink cooling kinetics

Bioink cooling kinetics were evaluated by first equilibrating freshly prepared bioinks at 37 °C and subsequently exposing them to a controlled room temperature environment (19.6 ± 0.2 °C). The temperature of the syringe containing the bioink was continuously monitored as a function of time.

Nonlinear regression analysis was performed using GraphPad Prism (version 9.0), and the goodness of fit was assessed using the coefficient of determination (R^2). For each bioink, the printing time window was defined as the time interval during which the bioink temperature remained within the predicted printing temperature window.

4.9. Validation of the predicted window

CAD models of a mesh (20x20 × 0.86 mm^3) and a quadrangular prism (10x10 × 2.52 mm^3) were printed at different temperatures and photographs were taken from top. Measurements of the structures were taken using ImageJ [40].

The spreading ratio was calculated according to the equation:

$$Spreading\ ratio = \frac{Thickness_{experimental}}{Thickness_{CAD}}$$

Where $Thickness_{experimental}$ is the thickness of the printed filaments in different sections of the structure and $Thickness_{CAD}$ is the theoretical thickness according to CAD.

The shape fidelity was calculated according to the equation:

$$Shape\ fidelity = \frac{A_{experimental}}{A_{CAD}}$$

Where $A_{experimental}$ is the area of the printed structure and A_{CAD} is the theoretical area according to CAD.

The printability ratio was calculated according to the equation:

$$Printability\ ratio = \frac{Perimeter^2}{16\,A}$$

Where *Perimeter* is the experimental perimeter and *A* is the experimental area of the structure.

The height accuracy was obtained by printing 10 x 10 × 10 mm3 prisms with a 22G nozzle using different bioinks within the printing temperature window (n = 3). Side-view images were taken immediately after printing and after 5, 15, 30, and 60 min, and the height of the structures was measured several times across the printed structure using ImageJ. The heigh accuracy was calculated according to the equation:

$$Height\ accuracy\ (\%) = \frac{Height_{t0}}{Height_{CAD}}\ x\ 100\%$$

Where $Height_{t0}$ is the mean height of the printed structure immediately after printing, and $Hight_{CAD}$ is the height of the CAD model (5 mm).

Height stability was calculated according to the equation:

$$Height\ stability\ (\%) = \frac{Height_{tX}}{Height_{t0}}\ x\ 100\%$$

Where $Height_{tx}$ is the mean height measured at a given time after printing.

4.10. Stability under incubation

CAD (cylinder 10 × 2.52 mm) structures were printed using bioinks **A1G6** and **A1G7** and were set under incubation in a mixture of DMEM:L-15 (1:1) culture media for different times (37 °C, 5% CO_2).Pictures were taken from top and side of the structure and measurements were taken using ImageJ. The diameter or the height of the structures after incubation relative to that before incubation was obtained and plotted as the degradation profile. Significant differences ($P < 0.05$) were determined by performing a one-way ANOVA with Tukey's multiple comparison tests were performed using Python.

4.11. Cell culture

Triple-negative breast cancer MDAMB231 cell line was provided by the group of Prof. João Conde from Nova Medical School. A suspension of MDAMB231 cells in Leibovitz's L-15 (L-15) medium supplemented with 15% (v/v) FBS and 1% (v/v) of Pen Strep (all from Thermo Fisher Scientific) was seeded in T75 culture flasks (75 cm^2 surface area) and incubated at 37 °C and 0 % CO2.

When the desired confluency was achieved (>70%), cells were detached from the surface by removing the medium, washing with PBS (7 mL), and incubating with trypsin enzyme (TrypLE® Express Enzyme 1X, Gibco) (2 mL) for 5 – 10 min at 37 °C, after which 5 mL of medium was added. The detachment of cells was verified using brightfield microscopy, using mechanical stress if required, and the concentration of cells in the suspension was determined using a Neubauer chamber under brightfield microscopy.

4.11.1. Bioink preparation

For biocompatibility experiments, gel **A1G7** was tested using MDAMB231 cells. **A1G7.MDAMB231** bioink was prepared in sterile conditions inside the flow hood and kept at 4 °C until used. Briefly, the hydrogel **A1G7** was warmed up to 37 °C 30 min and was added at 37 °C to a cell pellet containing the corresponding number of cells, and the cell pellet was carefully resuspended with a micropipette util a homogeneous suspension was observed macroscopically. The final cell concentration in the hydrogel was 1.9 × 10^6 cell/mL for biocompatibility experiments whereas 8 × 10^6 cell/mL to assess the viability after printing.

4.12. Biocompatibility

Aliquots of 100 μL were disposed over 96-well plates using a micropipette and left to stand at room temperature for 5 min until they solidified. 150 μL of a 100 mM CaCl2 solution was added to the wells containing the gel with cells and was incubated at room temperature for

1 min, after which the solution was removed, the gels were washed with PBS (1X) and were immersed in culture medium. Finally, the hydrogels were incubated at 37 °C and 5 % CO2 for 1 or 9 days. Hydrogels were stained with 150 μL of live/dead staining solution for 30 min at room temperature, after which the solution was removed, and gels were observed.

Cell viability was assessed by means of counting the number of live (green) and dead (red) cells in the images using ImageJ software, and was calculated according to the equation:

$$\textit{Cell viability}\ (\%) = 100\%\ \frac{n_{\textit{live cells}}}{n_{\textit{live cells}} + n_{\textit{dead cells}}}$$

Significant differences ($P < 0.05$) were determined by performing a one-way ANOVA with Tukey's multiple comparison tests were performed using Python.

4.13. Influence of the printing process on cell viability

Gel **A1G7.MDAMB231** was prepared in sterile conditions in the same way as in biocompatibility experiments but using a cell concentration of 8×10^6 cell/mL. The bioprinter was sterilized using 70% ethanol in water and placed inside the flow hood. The bioink was loaded into a 5 mL syringe at 37 °C and loaded into the bioprinter. A 5 mm diameter half-sphere design was printed in 6-well plates at a syringe temperature within the ideal printing temperature range, after which the constructs were left to stand at room temperature for 5 min, and were crosslinked by immersion in a 100 mM $CaCl_2$ solution for 1 min, washed with PBS, and immersed in L-15 culture medium before being incubated. After 24 h, the medium was removed, and the constructs were stained with live/dead staining as described previously. Constructs were imaged under confocal fluorescence microscopy and cell viability was calculated as described previously.

CRediT authorship contribution statement

Inês Anjos: Data curation, Investigation, Software. **Tânia Vieira:** Conceptualization, Investigation, Methodology, Resources, Writing – review & editing. **Luana Ventura:** Data curation, Investigation, Software. **Taslima Aktar:** Investigation. **Jorge Carvalho Silva:** Funding acquisition, Methodology, Resources. **Bárbara B. Mendes:** Methodology, Resources, Writing – review & editing. **João Conde:** Methodology, Resources, Writing – review & editing. **Luis Felipe Bolaños:** Software, Visualization. **Susete Fernandes:** Resources. **Catarina Leal:** Formal analysis, Investigation, Methodology, Resources, Software, Writing – review & editing. **João Paulo Borges:** Conceptualization, Funding acquisition, Methodology, Resources, Supervision, Writing – review & editing. **David Limón:** Conceptualization, Data curation, Formal analysis, Funding acquisition, Investigation, Methodology, Project administration, Software, Supervision, Visualization, Writing – original draft, Writing – review & editing.

Declaration of competing interest

The authors declare the following financial interests/personal relationships which may be considered as potential competing interests: David Limon Magana reports financial support was provided by LaCaixa Foundation. Joao Paulo Borges reports financial support was provided by Foundation for Science and Technology. Joao Conde reports financial support was provided by NOVA University Lisbon Comprehensive Health Research Centre. Catarina Leal reports financial support was provided by Foundation for Science and Technology. If there are other authors, they declare that they have no known competing financial interests or personal relationships that could have appeared to influence the work reported in this paper.

Acknowledgements

The work was supported by "La Caixa" Foundation through a Junior Leader Fellowship (ID100010434), FCT I.P. through projects of the AL Institute of Nanostructures, Nanomodelling and Nanofabrication-i3N (LA/P/0037/2020), CeFEMA, under the base and programmatic contract (UIDB/04540/2020), and Comprehensive Health Research Centre (UID/04923).

Appendix A. Supplementary data

Supplementary data to this article can be found online at https://doi.org/10.1016/j.polymertesting.2026.109138.

Data availability

Data will be made available on request.

References

[1] R. Augustine, S.N. Kalva, R. Ahmad, A.A. Zahid, S. Hasan, A. Nayeem, L. McClements, A. Hasan, 3D bioprinted cancer models: revolutionizing personalized cancer therapy, Transl. Oncol. 14 (4) (2021) 101015, https://doi.org/10.1016/j.tranon.2021.101015.
[2] C. Jensen, Y. Teng, Is it time to start transitioning from 2D to 3D cell culture? Front. Mol. Biosci. 7 (2020) 33, https://doi.org/10.3389/fmolb.2020.00033.
[3] B. Zhang, L. Gao, L. Ma, Y. Luo, H. Yang, Z. Cui, 3D bioprinting: a novel avenue for manufacturing tissues and organs, Engineering 5 (4) (2019) 777–794, https://doi.org/10.1016/j.eng.2019.03.009.
[4] A.C. Daly, M.E. Prendergast, A.J. Hughes, J.A. Burdick, Bioprinting for the biologist, Cell 184 (1) (2021) 18–32, https://doi.org/10.1016/j.cell.2020.12.002.
[5] B.B. Mendes, M. Gómez-Florit, A.G. Hamilton, M.S. Detamore, R.M.A. Domingues, R.L. Reis, M.E. Gomes, Human platelet lysate-based nanocomposite bioink for bioprinting hierarchical fibrillar structures, Biofabrication 12 (1) (2019) 015012, https://doi.org/10.1088/1758-5090/ab33e8.
[6] D. Limón, C. Jiménez-Newman, M. Rodrigues, A. González-Campo, D. B. Amabilino, A.C. Calpena, L. Pérez-García, Cationic supramolecular hydrogels for overcoming the skin barrier in drug delivery, ChemistryOpen 6 (4) (2017) 585–598, https://doi.org/10.1002/open.201700040.
[7] M.P. Lutolf, Spotlight on hydrogels, Nat. Mater. 8 (6) (2009) 451–453, https://doi.org/10.1038/nmat2458.
[8] M.B. Łabowska, K. Cierluk, A.M. Jankowska, J. Kulbacka, J. Detyna, I. Michalak, A review on the adaption of alginate-gelatin hydrogels for 3D cultures and bioprinting, Materials 14 (4) (2021) 858, https://doi.org/10.3390/ma14040858.
[9] P.S. Gungor-Ozkerim, I. Inci, Y.S. Zhang, A. Khademhosseini, M.R. Dokmeci, Bioinks for 3D bioprinting: an overview, Biomater. Sci. 6 (5) (2018) 915–946, https://doi.org/10.1039/c7bm00765e.
[10] A. Fatimi, O.V. Okoro, D. Podstawczyk, J. Siminska-Stanny, A. Shavandi, Natural hydrogel-based bio-inks for 3D bioprinting in tissue engineering: a review, Gels 8 (3) (2022) 3, https://doi.org/10.3390/gels8030179.
[11] R. Suntornnond, J. An, C.K. Chua, Bioprinting of thermoresponsive hydrogels for next generation tissue engineering: a review, Macromol. Mater. Eng. 302 (1) (2017) 1600266, https://doi.org/10.1002/mame.201600266.
[12] N. Soltan, L. Ning, F. Mohabatpour, P. Papagerakis, X. Chen, Printability and cell viability in bioprinting alginate dialdehyde-gelatin scaffolds, ACS Biomater. Sci. Eng. 5 (6) (2019) 2976–2987, https://doi.org/10.1021/acsbiomaterials.9b00167.
[13] S. El Moussaoui, F. Fernández-Campos, C. Alonso, D. Limón, L. Halbaut, M. L. Garduño-Ramirez, A.C. Calpena, M. Mallandrich, Topical mucoadhesive alginate-based hydrogel loading ketorolac for pain management after pharmacotherapy, ablation, or surgical removal in condyloma acuminata, Gels 7 (1) (2021) 1, https://doi.org/10.3390/gels7010008.
[14] X.B. Chen, A. Fazel Anvari-Yazdi, X. Duan, A. Zimmerling, R. Gharraei, N. K. Sharma, S. Sweilem, L. Ning, Biomaterials/bioinks and extrusion bioprinting, Bioact. Mater. 28 (2023) 511–536, https://doi.org/10.1016/j.bioactmat.2023.06.006.
[15] D. Chimene, K.K. Lennox, R.R. Kaunas, A.K. Gaharwar, Advanced bioinks for 3D printing: a materials science perspective, Ann. Biomed. Eng. 44 (6) (2016) 2090–2102, https://doi.org/10.1007/s10439-016-1638-y.
[16] T. Gao, G.J. Gillispie, J.S. Copus, A.K. Pr, Y.-J. Seol, A. Atala, J.J. Yoo, S.J. Lee, Optimization of gelatin–alginate composite bioink printability using rheological parameters: a systematic approach, Biofabrication 10 (3) (2018) 034106, https://doi.org/10.1088/1758-5090/aacdc7.
[17] S. Flores-Torres, O. Peza-Chavez, H. Kuasne, J.G. Munguia-Lopez, J. Kort-Mascort, L. Ferri, T. Jiang, C.V. Rajadurai, M. Park, V. Sangwan, J.M. Kinsella, Alginate–gelatin–Matrigel hydrogels enable the development and multigenerational passaging of patient-derived 3D bioprinted cancer spheroid models, Biofabrication 13 (2) (2021) 025001, https://doi.org/10.1088/1758-5090/abdb87.
[18] B. Sarker, R. Silva, N. Lang, R. Detsch, J. Kaschta, B. Fabry, A.R. Boccaccini, Alginate-based hydrogels with improved adhesive properties for cell

encapsulation, Int. J. Biol. Macromol. 78 (2015) 72–78, https://doi.org/10.1016/j.ijbiomac.2015.03.061.
[19] J.H.Y. Chung, S. Naficy, Z. Yue, R. Kapsa, A. Quigley, S.E. Moulton, G.G. Wallace, Bio-ink properties and printability for extrusion printing living cells, Biomater. Sci. 1 (7) (2013) 763, https://doi.org/10.1039/c3bm00012e.
[20] L. Ouyang, R. Yao, Y. Zhao, W. Sun, Effect of bioink properties on printability and cell viability for 3D bioplotting of embryonic stem cells, Biofabrication 8 (3) (2016) 035020, https://doi.org/10.1088/1758-5090/8/3/035020.
[21] Q. Li, B. Zhang, Q. Xue, C. Zhao, Y. Luo, H. Zhou, L. Ma, H. Yang, D. Bai, A systematic thermal analysis for accurately predicting the extrusion printability of Alginate–gelatin-based hydrogel bioinks, Int. J. Bioprint. 7 (3) (2021) 394, https://doi.org/10.18063/ijb.v7i3.394.
[22] B. Webb, B.J. Doyle, Parameter optimization for 3D bioprinting of hydrogels, Bioprinting 8 (2017) 8–12, https://doi.org/10.1016/j.bprint.2017.09.001.
[23] N. Paxton, W. Smolan, T. Böck, F. Melchels, J. Groll, T. Jungst, Proposal to assess printability of bioinks for extrusion-based bioprinting and evaluation of rheological properties governing bioprintability, Biofabrication 9 (4) (2017) 044107, https://doi.org/10.1088/1758-5090/aa8dd8.
[24] M.D. Giuseppe, N. Law, B. Webb, R.A. Macrae, L.J. Liew, T.B. Sercombe, R. J. Dilley, B.J. Doyle, Mechanical behaviour of alginate-gelatin hydrogels for 3D bioprinting, J. Mech. Behav. Biomed. Mater. 79 (2018) 150–157, https://doi.org/10.1016/j.jmbbm.2017.12.018.
[25] A. Ribeiro, M.M. Blokzijl, R. Levato, C.W. Visser, M. Castilho, W.E. Hennink, T. Vermonden, J. Malda, Assessing bioink shape fidelity to aid material development in 3D bioprinting, Biofabrication 10 (1) (2017) 014102, https://doi.org/10.1088/1758-5090/aa90e2.
[26] T. Gregory, P. Benhal, A. Scutte, D. Quashie, K. Harrison, C. Cargill, S. Grandison, M.J. Savitsky, S. Ramakrishnan, J. Ali, Rheological characterization of cell-laden alginate-gelatin hydrogels for 3D biofabrication, J. Mech. Behav. Biomed. Mater. 136 (2022) 105474, https://doi.org/10.1016/j.jmbbm.2022.105474.
[27] A. Ahmadi Soufivand, J. Faber, J. Hinrichsen, S. Budday, Multilayer 3D bioprinting and complex mechanical properties of alginate-gelatin mesostructures, Sci. Rep. 13 (1) (2023) 11253, https://doi.org/10.1038/s41598-023-38323-2.
[28] R. Chang, J. Nam, W. Sun, Effects of dispensing pressure and nozzle diameter on cell survival from solid freeform fabrication-based direct cell writing, Tissue Eng. 14 (1) (2008) 41–48, https://doi.org/10.1089/ten.a.2007.0004.
[29] A. Mondal, A. Gebeyehu, M. Miranda, D. Bahadur, N. Patel, S. Ramakrishnan, A. K. Rishi, M. Singh, Characterization and printability of sodium alginate -Gelatin hydrogel for bioprinting NSCLC co-culture, Sci. Rep. 9 (1) (2019) 19914, https://doi.org/10.1038/s41598-019-55034-9.
[30] D. Limón, C. Jiménez-Newman, A.C. Calpena, A. González-Campo, D.B. Amabilino, L. Pérez-García, Microscale coiling in bis-imidazolium supramolecular hydrogel fibres induced by the release of a cationic serine protease inhibitor, Chem. Commun. 53 (32) (2017) 4509–4512, https://doi.org/10.1039/C6CC09392B.
[31] Ö. Pekcan, S. Kara, Gelation mechanisms, Mod. Phys. Lett. B 26 (27) (2012) 1230019, https://doi.org/10.1142/S0217984912300190.
[32] S.M. Fitzsimons, D.M. Mulvihill, E.R. Morris, Denaturation and aggregation processes in thermal gelation of whey proteins resolved by differential scanning calorimetry, Food Hydrocoll. 21 (4) (2007) 638–644, https://doi.org/10.1016/j.foodhyd.2006.07.007.
[33] P. Atkins, J. de Paula, Atkins' Physical Chemistry, ninth ed., Oxford University Press, 2010.
[34] D.L. Nelson, M.M. Cox, Lehninger Principles of Biochemistry, fifth ed., W.H. Freeman and Company, 2008.
[35] S.R. Derkach, N.G. Voron'ko, N.I. Sokolan, D.S. Kolotova, Y.A. Kuchina, Interactions between gelatin and sodium alginate: UV and FTIR studies, J. Dispersion Sci. Technol. 41 (5) (2020) 690–698, https://doi.org/10.1080/01932691.2019.1611437.
[36] A.C. Daly, S.E. Critchley, E.M. Rencsok, D.J. Kelly, A comparison of different bioinks for 3D bioprinting of fibrocartilage and hyaline cartilage, Biofabrication 8 (4) (2016) 045002, https://doi.org/10.1088/1758-5090/8/4/045002.
[37] A. Schwab, R. Levato, M. D'Este, S. Piluso, D. Eglin, J. Malda, Printability and shape fidelity of bioinks in 3D bioprinting, Chem. Rev. 120 (19) (2020) 11028–11055, https://doi.org/10.1021/acs.chemrev.0c00084.
[38] M.K. Kim, W. Jeong, S.M. Lee, J.B. Kim, S. Jin, H.-W. Kang, Decellularized extracellular matrix-based bio-ink with enhanced 3D printability and mechanical properties, Biofabrication 12 (2) (2020) 025003, https://doi.org/10.1088/1758-5090/ab5d80.
[39] M.-Y. Shie, J.-J. Lee, C.-C. Ho, S.-Y. Yen, H.Y. Ng, Y.-W. Chen, Effects of gelatin methacrylate bio-ink concentration on mechano-physical properties and human dermal fibroblast behavior, Polymers 12 (9) (2020) 1930, https://doi.org/10.3390/polym12091930.
[40] C.A. Schneider, W.S. Rasband, K.W. Eliceiri, NIH image to ImageJ: 25 years of image analysis, Nat. Methods 9 (7) (2012) 671–675, https://doi.org/10.1038/nmeth.2089.